JOURNAL OF MATERIALS SCIENCE 32 (1997) 5335–5346

Fracture resistance of polyblends and polyblend matrix composites

Part I *Unreinforced and fibre-reinforced nylon 6,6/ABS polyblends*

S. V. NAIR*, S-C. WONG‡
Department of Mechanical Engineering, University of Massachusetts, Amherst, MA 01003, USA

L. A. GOETTLER
Vydyne Tech Center, Monsanto Company, Cantonment, FL 32533, USA

The deformation behaviour and the fracture resistance of a range of nylon 6,6/ABS alloys of varying composition both with and without the presence of glass fibres were investigated. The deformation behaviour was characterized by careful measurements of the volumetric strain during tensile tests in order to understand the relative roles of cavitation and shear yielding in these materials. The fracture resistance was investigated in detail in the fracture mechanics sense by characterizing the *J*-integral fracture initiation toughness. In materials exhibiting stable crack growth, a new parameter, namely, the plateau value of the *J*-integral fracture resistance curve, was measured directly and represented the resistance of the material to stable crack growth. The results showed that the relationship between the deformation behaviour and fracture resistance was related to the extent of damage that developed in the crack-tip zone. Substantial additional toughening was developed during the crack extension stage both in the presence and absence of glass fibres. Glass fibres were found to promote shear yielding and, as a result, enhance both the fracture initiation as well as the fracture propagation resistance of the nylon 6,6/ABS alloys.

1. Introduction

A widely employed strategy for improving the toughness of single thermoplastics has involved the addition of an elastomeric phase to the thermoplastic. Current understanding is that internal cavitation of the elastomeric phase can relieve stress triaxiality ahead of flaws, thereby enhancing localized shear deformation [1–8]. A disadvantage of the reliance on an elastomeric phase for toughening is that such additions can also reduce modulus and strength which are important benchmarks for acceptable material performance.

In comparison with studies of elastomer phase toughening of single polymers, the toughening behaviour of polymer–polymer blends or alloys (polyblends) and polyblend matrix composites containing an elastomeric phase, has received little attention. In these systems, the toughening role of the elastomeric component is accompanied by the strengthening and stiffening role of one or more rigid phases which includes other rigid polymer phases in the unreinforced polyblends and, in addition, the rigid reinforcing phase in the composites.

Therefore, in this paper, Part I, and the other five papers of the series [9–13], we explore the use of polyblends containing an elastomeric phase and such blends reinforced with glass fibres as a route to obtaining both a tough as well as a strong and stiff polymer. In the first four papers, we focus on nylon 6,6/acrylonitrile butadiene styrene (ABS) alloys. Here, in addition to the presence of a rubber phase, the unreinforced materials contain the rigid styrene acrylonitrile (SAN) polymer and the rigid nylon 6,6 polymer, while the reinforced materials contain, in addition, the rigid glass fibre-reinforcing phase. In the next two papers we focus on polycarbonate (PC)/ABS blends and PC/ABS blends reinforced with glass fibres. The rigid phases in these latter blends are PC, SAN and glass fibres.

The main focus in these papers is the fundamentals of fracture resistance when the elastomeric phase, here the rubber phase, is present in association with other rigid phases, namely the polymer rigid phase(s) and the glass fibres. The fundamentals of the role of the rubber phase and the rubber phase type, the rigid polymer phase and the glass fibres on fracture

*Author to whom all correspondence should be addressed.
‡*Present address*: Center for Advanced Materials Technology, Department of Mechanical and Mechatronic Engineering, The University of Sydney, Sydney, NSW 2006, Australia.

0022–2461

resistance will be explored in detail. The approach used to understand fracture fundamentals is to employ a rigorous fracture mechanics approach. In this context two important parameters of toughening were explored. One was the fracture initiation toughness and the other was the additional toughening that could be obtained as a result of crack extension which we term the fracture propagation toughness. The fracture propagation toughness is related to the material *R*-curve, or resistance curve, behaviour.

In this first of the six papers, a range of nylon 6,6/ABS alloys ranging from pure nylon 6,6 to pure ABS have been studied both in the unreinforced as well as the glass fibre-reinforced composites. We considered two aspects. The first was the role of ABS or nylon 6,6 and of the glass fibres in influencing the deformation behaviour of the major phase, and second was their role in influencing the fracture resistance. In studying the former we have made careful measurements of the dilatational component of deformation in these materials and in studying the latter we have made measurements of the *J*-integral toughness, both initiation as well as propagation components of toughness. All of these measurements are related to the microstructure of these materials. We have also varied the extent of compatibilization between the nylon 6,6 and the ABS phase in a preliminary effort to understand the role and the nature of the nylon 6,6/ABS interface on the fracture resistance of the polymer alloy.

The nylon/ABS system was originally invented by Monsanto Chemical Company [14–18], who demonstrated an increase in the impact toughness of nylon 6 by addition of ABS and a suitable compatibilizer. Subsequent studies by Paul and co-workers [7, 19–22] support toughening of nylon 6 by ABS. The toughening mechanism was apparently one where cavitation occurred in the rubbery phase within the ABS, followed by shear yielding of the nylon 6 phase [7].

We emphasize here the use of the *J*-integral fracture mechanics parameter for studying toughness of tough polymers wherein the load–displacement records of pre-cracked samples exhibit non-linearity. Furthermore, we have used a new J_{ss} parameter as a measure of the overall toughness which includes both the initiation as well as the fracture propagation toughness components. J_{ss} is essentially the plateau, or steady-state, value of the fracture resistance, J_R. The use of J_{ss} for polymer materials has been demonstrated previously [23, 24]. The J_{ss} parameter has also been applied to describe the fracture resistance plateau in ceramic composites [25, 26].

2. Experimental procedure

2.1. Materials

The polymer materials studied were poly(hexamethylene adipamide)/acrylonitrile-butadiene-styrene copolymer or nylon 6,6/ABS alloys. The ABS and dried nylon 6,6 materials were compounded together with a maleic anhydride-type compatibilizer at weight ratios of 0/100, 20/80, 50/50, 80/20, and 100/0 in an American Leistritz twin-screw extruder. The ABS comprised about 14 wt % grafted rubber in a 75/25 SAN copolymer matrix [23]. The extruded alloys were then dried in a vacuum oven for at least 24 h before being injection moulded into 6.35 mm thick Izod bars and tensile specimens (ASTM D638 type I) with a thickness of 3.18 mm for both the unreinforced and fibre-reinforced materials. The moulding temperature for the unreinforced alloys was increased as the nylon 6,6 content increased. While a compatibilizer content of 4 wt % was used in all the materials, 20/80 nylon 6,6/ABS alloys were also studied in the presence of 7 and 10 wt % compatibilizer content. As mentioned, this was done in order to understand the role of the nature of the nylon 6,6/ABS interface on fracture resistance.

Glass fibre-reinforced nylon 6,6/ABS composites were made by pre-compounding glass fibres at 16 vol % of the total filled polymer. The glass fibre used was a product of Schuller Mats and Reinforcements named Star Stran 702 with a filament diameter of 13 μm. These fibres were provided by the manufacturer with a proprietary surface condition deemed to be nylon 6,6 compatible. In the composite, the moulding temperature was increased about 20 °C above that of the unreinforced nylon 6,6/ABS to improve the flow of the glass fibres. The fibres were oriented and broken down by the melt-flow process, yielding a partially oriented system with variable fibre lengths. The moulding pressure for the composite was also increased to force the material to fill the mould completely. To avoid moisture- and light-degradation effects, after injection moulding all the specimens were sealed first in PE film and then in aluminized paper until they were tested.

2.2. Microscopy

Fracture surfaces of the materials studied were examined with a Jeol scanning electron microscope (SEM) after loading single-edge notched bend (SENB) specimens at 5 mm min^{-1} until fracture. The phase morphology was also characterized by SEM on a polished surface of the specimen in a direction parallel to the moulding direction. Samples were coated with gold–palladium prior to examination. The microstructures of the unreinforced SENB samples were cut for transmission electron microscopy (TEM) from the centre, parallel and perpendicular to the flow directions. The specimens were cryo-sectioned with a diamond knife and sections were collected on a 400 mesh TEM grid. The grids with the sections were then stained in 1% phosphotungstic acid and benzyl alcohol for 30 min to reveal the nylon 6,6 phase followed by 1% osmium tetroxide for 30 min to reveal the butadiene particles.

2.3. Mechanical properties

Tensile tests were carried out according to ASTM D638 on a computer-controlled Instron model 1321 servohydraulic testing machine. Five specimens of each of the different compositions were tested. The displacement rate used for all tensile testing was 5 mm min^{-1}. All tests were carried out at room temperature upon removal of specimens from the specimen storage bags.

The J-integral initiation toughness for the specimens was determined by standard ASTM method E813 using a three-point bend specimen with a span-to-width, $L/W = 4$ ($L = 5.08$ cm, $W = 1.27$ cm, and thickness, $B = 0.64$ cm). The single-edge initial notch of each specimen was created by a diamond saw cut. Pre-cracks were made by inserting a fresh microtome blade into a machined slot, and the crack-to-width ratio, a/W, was limited to 0.45–0.55 for all tests. The specimen thickness values needed for valid plane strain toughness measurements were also checked according to the ASTM recommended values of

$$B \geqslant \frac{25 J_Q}{\sigma_y} \tag{1}$$

where a is the precrack length, B is the thickness, W is the width of the specimen and J_Q, σ_y are the toughness and the material yield stress, respectively. The specimens were then loaded in an Instron model 1321 servohydraulic testing machine at a rate of 5 mm min^{-1} at room temperature. After unloading, the specimens were then placed in a bath of liquid nitrogen for at least 1 min and then fast fractured. The amount of crack growth, Δa, was measured using an optical stereo microscope and the J-integral fracture resistance, J_R, was determined using the equation

$$J_R = \frac{2U}{Bb} \tag{2}$$

where U is the area under load–displacement curve, and b is the ligament length. The initiation toughness, J_{IC}, was determined by intersection of the J_R–Δa curve with the blunting line ($J = 2\sigma_y \Delta a$, where σ_y = yield stress) solution at 0.2 mm offset.

In order to measure the J steady-state toughness, J_{ss}, two identical three-point bend specimens with slightly different initial crack lengths were used. The specimens were then precracked and loaded in a similar fashion as specified by the ASTM method E813 at a rate of 5 mm min^{-1} until fracture. The load–load-line displacement (P–δ) curves were measured for each set of specimens. A schematic illustration of the P–δ curves for the two specimens is shown in Fig. 1. Note that at $\delta = \delta_{ss}$, the two curves come together. This indicates the attainment of the plateau value of the fracture resistance. As demonstrated by Hashida and Li [25], the value of the J-integral for a given value of δ can be expressed as the area, $A(\delta)$, between the P–δ curves for the two specimens with initial crack size difference, Δa, divided by the specimen thickness, B, and Δa

$$\begin{aligned} J_{ss} &= \int_0^{\delta_{ss}} \sigma(\delta)\, d\delta \\ &= \frac{1}{a_2 - a_1} \int_0^{\delta_{ss}} \left(\frac{P_1}{B_1} - \frac{P_2}{B_2} \right) d\delta \\ &= \frac{A(\delta_{ss})}{B \Delta a} \end{aligned} \tag{3}$$

where a_1, a_2, P_1 and P_2 are the initial crack lengths and applied loads of the two specimens, respectively. Plane strain thickness requirements for the J_{ss} values were also checked on the basis of Equation 1, where J_Q was set equal to J_{ss}.

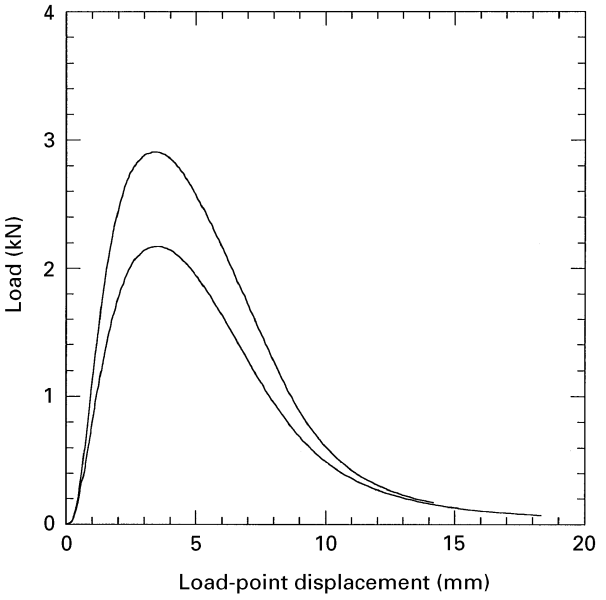

Figure 1 The load–displacement, P–δ, curves for two specimens with two different crack lengths. The top curve is for the shorter crack length that has a lower compliance. The energy dissipated reaches a maximum value when the two curves come together. This corresponds to attaining the plateau value of the fracture resistance curve.

2.4. Dilatational strain measurements

To investigate the deformation mechanism of each individual blend composition, dilatational strain measurements of unreinforced and fibre-reinforced nylon 6,6/ABS alloys were conducted. The dilatational strains were measured using a computer-controlled Instron 4202 system at a constant crosshead speed of 5 mm min^{-1}. Highly sensitive clip-on extensometers were used to monitor strains in the longitudinal and transverse directions. The thickness strain and the width strain were assumed to be equal. Three specimens of each material were tested and the dilatational strains of the deformed samples were then calculated from [27]

$$\frac{\Delta V}{V} = (1 + \varepsilon_x)(1 + \varepsilon_z)^2 - 1 \tag{4}$$

where ε_x denotes the strain in the loading direction and ε_z denotes the strain in the lateral direction. The true stress, σ, of each sample was obtained from

$$\sigma = \frac{P}{W_0 T_0 (1 - \varepsilon_z)^2} \tag{5}$$

where P is the applied load, W_0 and T_0 are the original width and thickness, respectively. It is generally known that the technique of tensile dilatometry provides a volume dilatation slope that is indicative of dilatational plasticity. This slope is the slope of the volumetric strain versus the axial strain.

3. Results and discussion

3.1. Microscopy

The microstructure of the unreinforced alloys contained two principal phases, namely, the ABS and

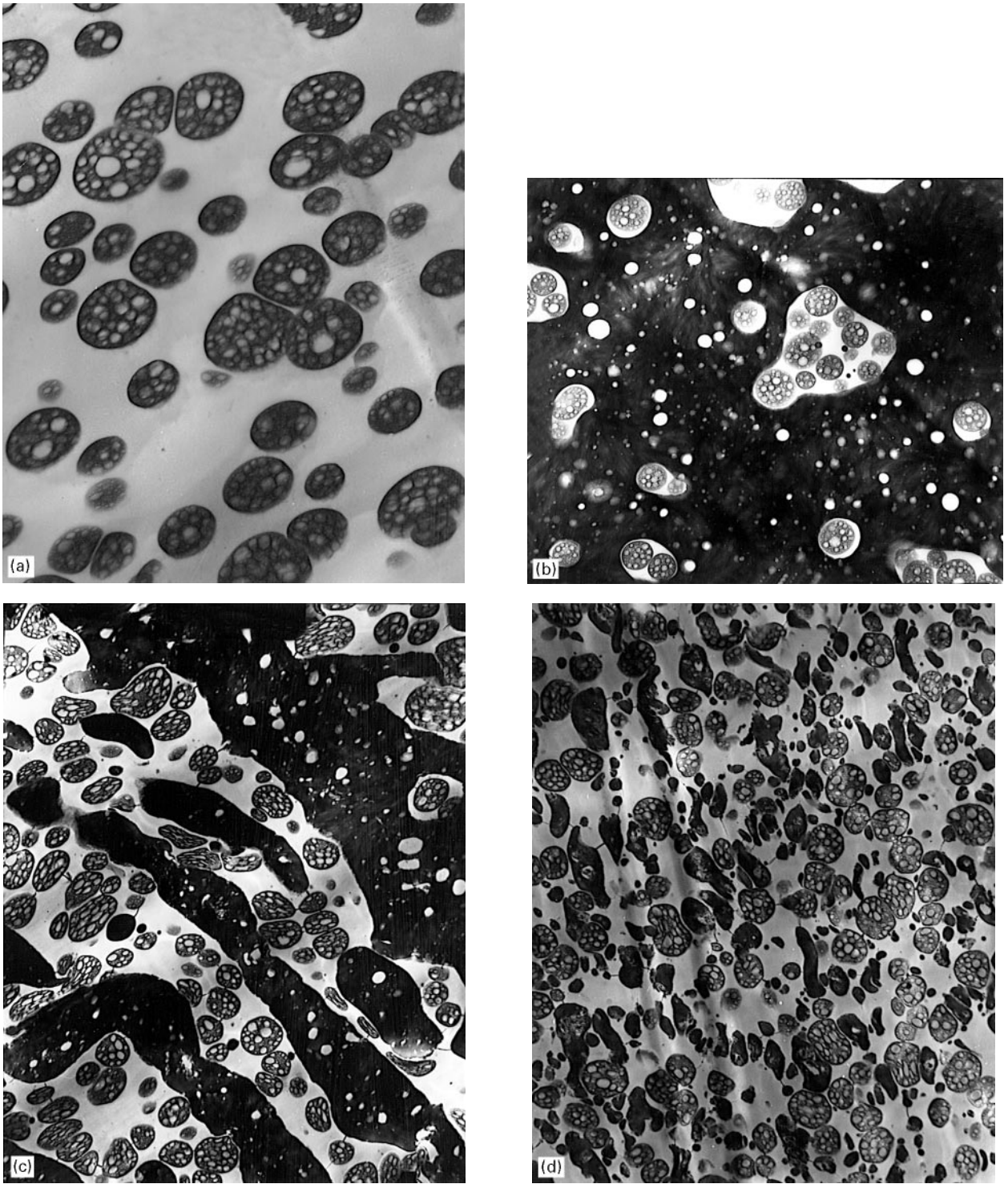

Figure 2 Transmission electron micrographs for (a) pure ABS, (b) 80/20 nylon 6,6/ABS, (c) 50/50 nylon 6,6/ABS and (d) 20/80 nylon 6,6/ABS. See text for discussion.

nylon 6,6 phases. The pure ABS phase, see Fig. 2a, contains a dispersion of relatively spherical butadiene particles approximately in the range 0.3–1.5 μm diameter. In blends of ABS with nylon 6,6, three contrasting microstructures were observed: (i) where the ABS phase was discontinuous and embedded in a nylon 6,6 resin, see Fig. 2b; (ii) where the two phases were co-continuous, Fig. 2c; (iii) where the nylon 6,6 was the discontinuous phase in ABS, see Fig. 2d.

For the 80/20 nylon 6,6/ABS system, where ABS was the discontinuous phase, see Fig. 2b, the size of the ABS phase varied between 1 and 5 μm, with several of the largest segments containing multiple embedded butadiene particles. The ABS regions containing multiple butadiene particles also had very complex shapes. In addition to the ABS phase, smaller white dispersions of the brittle SAN phase were also observed.

In the unreinforced 20/80 case, Fig. 2d, the discontinuous dark nylon 6,6 phase in ABS had an elongated morphology which, as will be seen, had a bearing on the fracture resistance results.

TEM was not performed in the fibre-reinforced nylon 6,6/ABS, owing to the difficulty of obtaining thin sections of materials containing glass fibres. Hence the microstructures of the composites were inferred from the fracture surfaces. It was found (see

Fig. 12a and b, below), that the nylon 6,6 phase was discontinuous and elongated in the 20/80 nylon 6,6/ABS matrices while the ABS phase was discontinuous in the 80/20 nylon 6,6/ABS matrices similar to that for the unreinforced system. However, we did not find evidence of co-continuity in the 50/50 nylon 6,6/ABS matrix, suggesting that co-continuity may have occurred at a different composition in the composite matrix as compared to that in the unreinforced polyblend.

3.2. Tensile properties

The tensile stress–strain curves are shown for the unreinforced alloys in Fig. 3. Pure nylon 6,6, as was shown previously [28] exhibited a two-stage behaviour, with two plateau regions. The previous study [28] showed that the first plateau was a result of crystalline plasticity, whereas the second plateau was a result of necking plasticity. It is evident from the figure that this two-stage behaviour was lost once the ABS content was greater than 20%. In pure ABS the deformation behaviour is known to be governed by a substantial dilatational component as evidenced by observed stress whitening [2]. Qualitatively, the addition of ABS appears to have changed the deformation behaviour from the more deviatoric plasticity of nylon 6,6 to the more dilatational plasticity of ABS. This is further addressed in the next section.

Graphs of the tensile strengths of the blends as a function of nylon 6,6 content (Fig. 4) show that while the strength increases linearly with nylon 6,6 content for the unreinforced case, evidence of positive synergism can be observed in the fibre-reinforced alloys. The strengths of the intermediate blend matrix composite deviate positively from the linear-additive law and are greater than those of both reinforced ABS and reinforced nylon 6,6. The strength increase due to fibre additions ranges from around 1.5 for pure nylon 6,6 matrices to about 3 for pure ABS matrices. The former

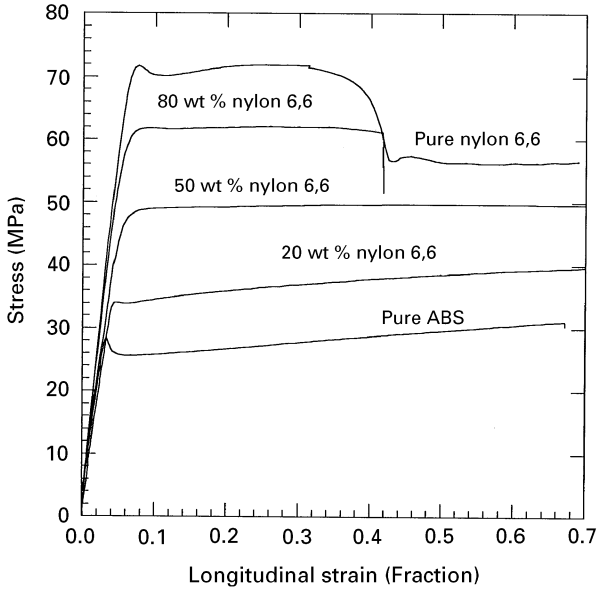

Figure 3 Tensile stress–strain curves for the unreinforced nylon 6,6/ABS alloys.

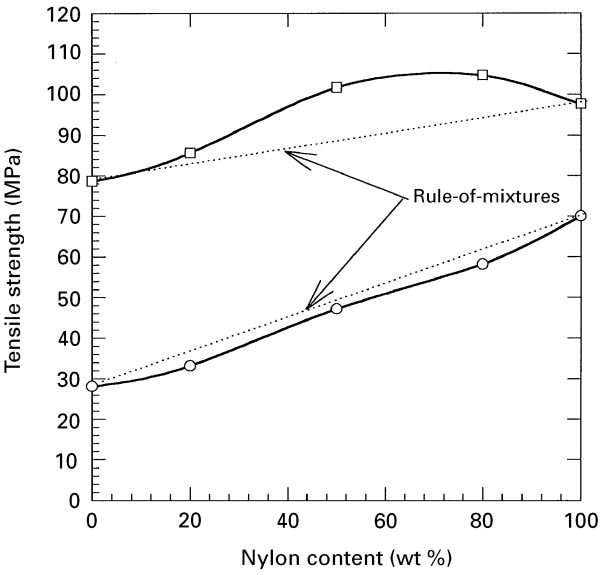

Figure 4 Tensile strength versus alloy composition for (○) unreinforced and (□) fibre-reinforced alloys.

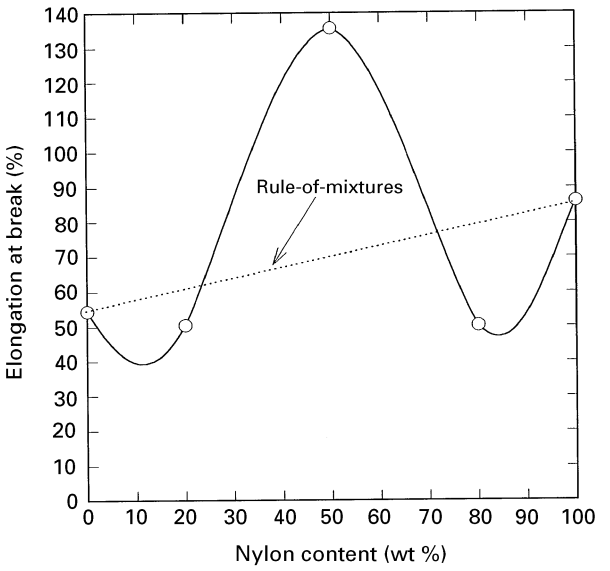

Figure 5 Strain to failure versus alloy composition for unreinforced alloys.

contains no rubber phase while the latter contains the maximum total rubber phase content. There appeared to be a somewhat greater strength increase due to fibres when the rubber phase was present.

The average tensile ductility is maximum for the 50/50 unreinforced alloy (Fig. 5), indicating substantial positive synergism that results from co-continuity of the nylon 6,6 and the ABS phases; however, this does not translate into improved ductility in the fibre-reinforced 50/50 alloy. Fig. 6 shows the average strain at break of the fibre-reinforced alloys. Evidently, introduction of fibres into the alloy system drastically reduced the ductility, compare Figs 5 and 6. Yielding prior to fracture was generally observed in 0/100, 80/20, 100/0 nylon 6,6/ABS alloys reinforced with 16 vol % glass fibres, whereas the 20/80 and 50/50 nylon 6,6/ABS fibre-reinforced polyblend failed predominantly by brittle pre-yield failure.

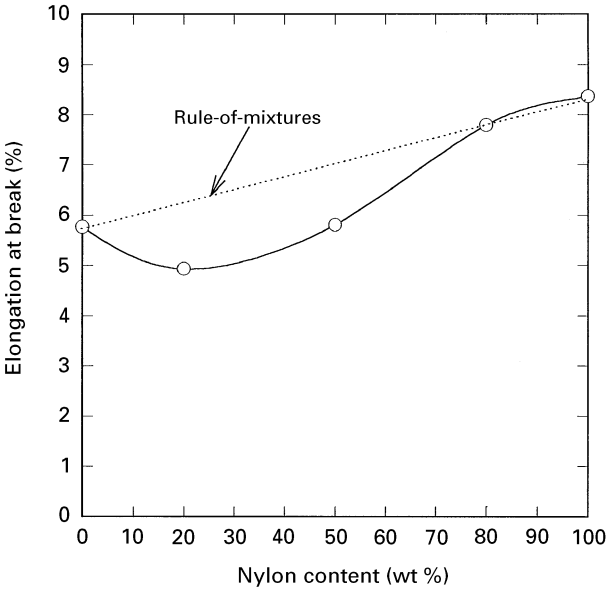

Figure 6 Strain to failure versus matrix alloy composition for fibre-reinforced alloys.

3.3. Tensile dilatometry

An example of the volumetric strain versus longitudinal axial strain for the unreinforced 20/80 nylon 6,6/ABS alloy is shown in Fig. 7a, where this result is plotted along with the true stress–strain curve. The corresponding result for the alloy with fibre reinforcement is shown in Fig. 7b. Although the bulk of the dilatational strain develops in the plastic region of the stress–strain curve, it is clear that, both with and without fibre reinforcements, the onset of cavitational strain begins in the elastic region of the tensile test prior to general yielding. This is consistent with the previously proposed theory [1–8] that cavitation is the precursor to shear yielding. The volume dilatation slope defined in the experimental section and which is indicative of the extent of dilatational deformation is shown in Fig. 8 for the unreinforced polyblends and the composites. A decrease in the volume dilatational slope means either that the dilatational strain per unit strain was reduced and/or that the deviatoric strain per unit strain was increased. The opposite would be true if the volume dilatational slope increased. In other words, the slope is a measure of the dilatational deformation component relative to the deviatoric deformation component.

For the unreinforced polyblends, as Fig. 8 indicates, the volume dilatational slope decreased as nylon 6,6 was added to ABS and approached essentially negligible values in the limit of pure nylon 6,6. In fact some negative values were also observed for pure nylon 6,6 which has been suggested to be the result of strain-induced crystallinity within the shear zone in neat nylon 6,6 [29]. The general decrease in the dilatational slope is consistent with the different deformation mechanisms in pure ABS and pure nylon 6,6. In ABS, dilatational strains can be induced by rubber cavitation which, in turn, enhances shear yielding in the surrounding SAN. In pure nylon 6,6, a detailed study [28] has shown that deformation is purely of a devi-

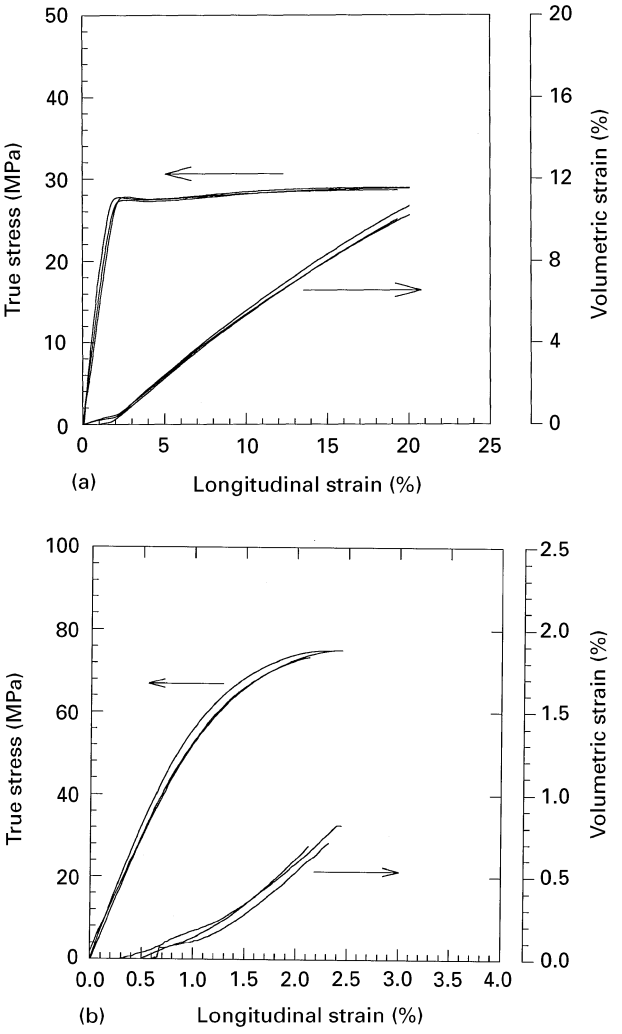

Figure 7 Volumetric strain versus axial strain plotted along with the true stress–strain curve for (a) unreinforced 20/80 nylon 6,6/ABS and (b) fibre-reinforced 20/80 nylon 6,6/ABS alloy.

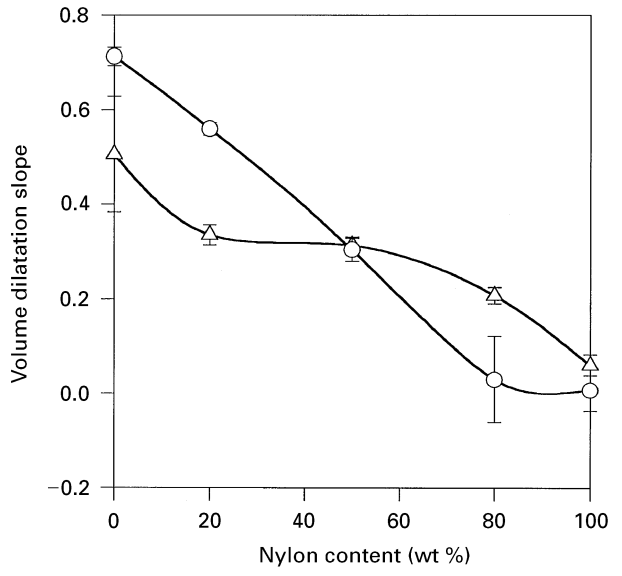

Figure 8 Comparison of the volume dilatational slope versus alloy composition for the (○) unreinforced and (△) fibre-reinforced alloys.

atoric nature associated with twinning mechanisms in the crystalline regions. The decrease in volume dilatational slope with nylon 6,6 volume fraction is roughly linear, as expected on the basis of a rule-of-mixtures

type of behaviour. This meant that the nylon 6,6 did not significantly alter the extent of dilatational and/or shear plasticity in the surrounding ABS phase.

It is insightful to observe the role played by fibres on deformation mechanisms. Fig. 8 shows that, except for the case of the 80/20 nylon 6,6/ABS, addition of fibres to the polyblend either decreased or did not significantly alter the volume dilatational slope. Assuming that the fibres themselves being elastic have essentially a zero dilatational slope, the predicted value of the dilatational slope for the composite when corrected for the matrix volume fraction ($=0.84$) is $0.84 \times$ (slope for unreinforced). On this basis, the fibres were seen significantly to reduce the slope for the matrix (when compared to the unreinforced polyblend) for the ABS-rich polyblends but increase the slope for the nylon 6,6-rich polyblends. It is argued that the decrease in the matrix dilatational slope for the ABS-rich alloys as a result of the presence of the fibres derives from an enhancement of the shear plasticity by fibres. Direct evidence for this was presented previously by Nair *et al.* [30, 31]. More recently, Shiao *et al.* [28] also showed that the fibres behave much the same way as rubber particles, in that they reduce local stress triaxiality and thereby enhance localized shear yielding, resulting in toughness trends with fibre volume fraction that were remarkably similar to trends found when rubber particles were added. This reduction in stress triaxiality is because of the high shear stress values in the matrix surrounding the fibres developed when the load is transferred from the matrix to the fibres. Implicit in the development of these high shear stresses is an adequately strong fibre/matrix interface. Supportive evidence for a good interface is presented in the next section.

In the nylon 6,6-rich polyblends, addition of fibres increased the dilatational deformation component relative to the deviatoric or shear component. This result could only be attributed to the fact that in the nylon 6,6-rich alloys there was extensive debonding between the ABS and nylon 6,6 phases (see next section). Apparently, the complex interaction between the resulting damage and the stress concentrations at fibres resulted overall in an increase in the triaxiality of deformation. As we will show later (see next section), fibre-reinforced composites with nylon 6,6-rich matrices exhibited no stable crack growth, whereas substantial stable crack growth was observed for ABS-rich matrices.

3.4. Fracture initiation toughness

We focus first on the fracture initiation toughness for the case of the unreinforced and fibre-reinforced polyblends, results for which are shown in Fig. 9. It was observed that the toughness values of the unreinforced polyblends were lower than those given by the corresponding rule-of-mixtures line, in other words there was a negative synergism in the toughness. The toughest polyblend appeared to be when both nylon 6,6 and ABS were co-continuous, as in the 50/50 composition case, although the toughness of this alloy was still lower than predicted by the rule of mixtures.

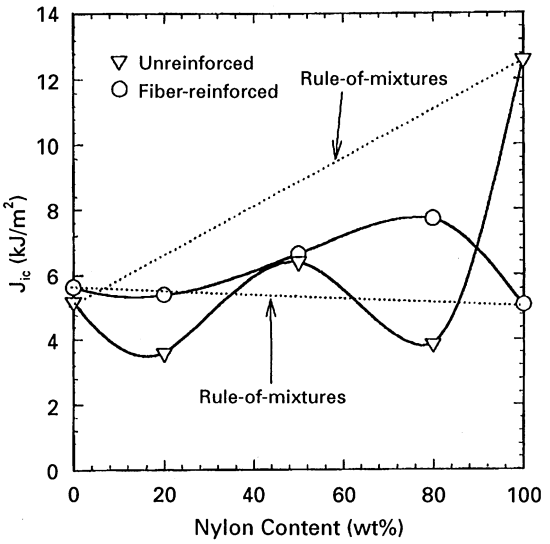

Figure 9 Fracture initiation toughness, J_{IC}, versus alloy composition for both the (▽) unreinforced and (○) fibre-reinforced alloys.

The tensile dilatometry results need to be applied with caution to interpret the toughness results, because uniaxial conditions underestimate the hydrostatic stresses at crack tips. Also the sharp stress gradients at crack tips are not encountered under uniaxial conditions. If the crack tip factors are not accounted for, then toughness as a function of composition should follow the trend dictated by the volume dilatational results of Fig. 9. That is, the toughness should increase going from ABS to nylon 6,6 roughly in a linear fashion, because the extent of shear deformation relative to volumetric deformation increased. Thus a beneficial effect of the crack tip should lead to positive synergism and a deleterious effect of the crack tip should lead to negative synergism. Accordingly, the fracture toughness results of Fig. 10 which showed negative synergism at all composition levels, suggested that in the presence of the crack tip, embrittlement effects were important. We discuss these effects below.

In the ABS-rich polyblends, toughness decreased, although the nylon 6,6 phase overall increased the relative extent of shear deformation in uniaxial tests. A factor associated with the crack-tip hydrostatic stress state and the crack-tip stress gradient is the tendency for internal fracture initiation within the crack-tip plastic zone through debonding at second phase/matrix interfaces. Experimental evidence of nylon 6,6/ABS debonding can be observed on the fracture surfaces, see Fig. 10a, for the case of the 20/80 nylon 6,6/ABS alloy which shows debonded and elongated nylon phase particles on the fracture surface. Such damage formation can enhance secondary fracture initiation in the plastic zone and lower toughness. Debonding at nylon 6,6 particle/ABS matrix interfaces is consistent with the larger modulus of the nylon 6,6 when compared with the ABS phase.

Consistent with the above discussion we found that when the ABS-to-nylon compatibilizer content was increased in order to obtain a stronger ABS/nylon 6,6 interface the fracture initiation toughness substantially

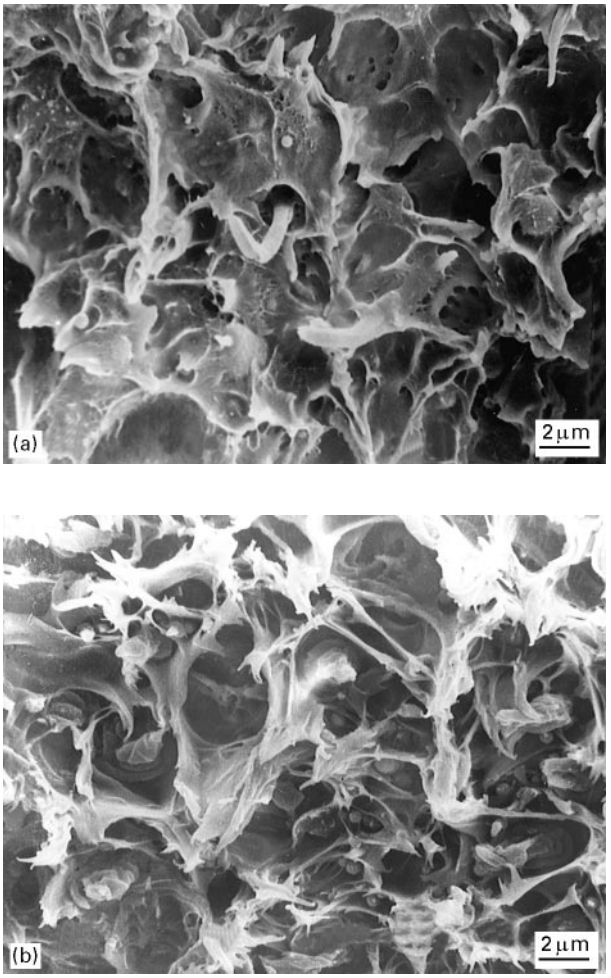

Figure 10 Scanning electron micrographs of fracture surface for 20/80 and 80/20 nylon 6,6/ABS alloys. (a) 20/80 alloy showing debonded and pulled out nylon phase. (b) 80/20 alloy showing extensive debonding between the discontinuous ABS phase and the nylon 6,6 matrix.

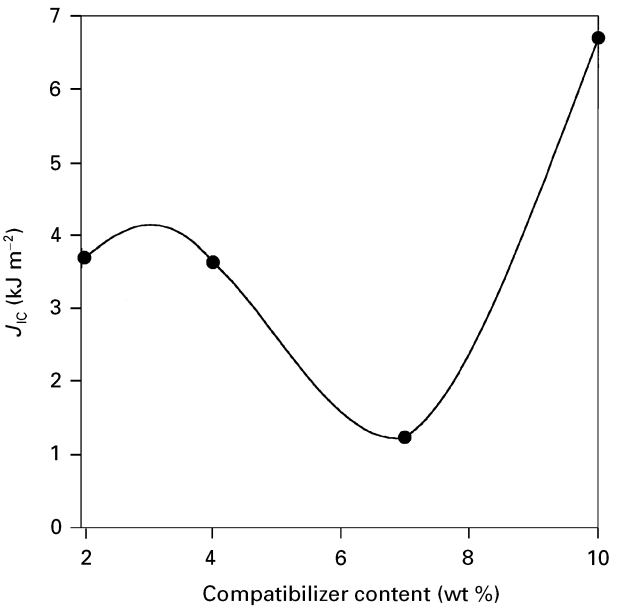

Figure 11 Fracture initiation toughness of the 20/80 nylon 6,6/ABS alloys as a function of the compatibilizer content.

increased, see Fig. 11. Indeed, at the highest compatibilizer content of 10%, the fracture toughness was above the rule-of-mixtures line, showing that positive synergism was achieved.

In the nylon 6,6-rich polyblends, the toughness was substantially less than predicted by the rule-of-mixtures. In this material also, extensive debonding between the discontinuous ABS and nylon 6,6 was observed, see Fig. 10b. The extensive debonding here we attribute to the non-uniform microstructure of the ABS. As previously pointed out, many of the ABS particles were large and contained several rubber particles. A second factor promoting damage in the plastic zone was the presence of a significant amount of free SAN without the rubber phase, as was shown in Fig. 3. SAN has a significantly higher modulus than nylon 6,6 and consequently can act as a strong stress concentrator. As expected, when toughness is controlled by internal secondary fracture or cracking within the crack-tip plastic zone, toughness is increasingly sensitive to microstructural variations.

It is important to point out that the motivation for adding ABS to nylon 6,6 was the anticipation of positive synergism in this case. That is, although addition of ABS enhanced dilatational plasticity in favour of shear plasticity in uniaxial tension as was shown in Fig. 8, at crack tips ABS can potentially lower the high local hydrostatic stresses and thereby promote enhanced localized plasticity, as has been proposed previously [8]. This is because ABS contains the cavitating rubber phase. Cavitation of the rubber phase in the high triaxial stress field of the crack tip can relieve the triaxiality and promote additional shear deformation in the surrounding nylon 6,6 phase. Apparently such cavitation enhanced plasticity and toughening did not take place when ABS was added to nylon 6,6 because of the dominance of damage in the plastic zone by ABS/matrix debonding effects.

In contrast with the case wherein one of the two polymer alloy components was discontinuous, toughness was clearly improved when the two components were co-continuous, see Fig. 9. The toughness approached the rule-of-mixtures values for this case but was still less than the averaged prediction. Evidently at crack tips, even for this microstructure, embrittlement effects lowered the toughness below the average value predicted on the basis of a uniaxial stress state.

We now address the fracture initiation toughness in the fibre-reinforced composites. Note from Fig. 9 that the composite toughness was always equal to or greater than the toughness of the corresponding unreinforced material except for the case of pure nylon 6,6. The maximum toughness increase was by about a factor of two for 80/20 nylon 6,6/ABS. For the case of pure nylon 6,6 the toughness was drastically lowered by the addition of glass fibres. As for the unreinforced alloys we examine the toughness trends in the ABS-rich and the nylon 6,6 rich regimes with respect to the deformation mechanism results of Fig. 8.

In the ABS-rich regime, as was discussed, fibres appeared to enhance shear plasticity in uniaxial tests. Apparently, this enhancement was operative in the crack-tip region as well, because, consistent with this, the fracture toughnesses of the fibre-reinforced ABS and the fibre-reinforced 20/80 nylon 6,6/ABS were

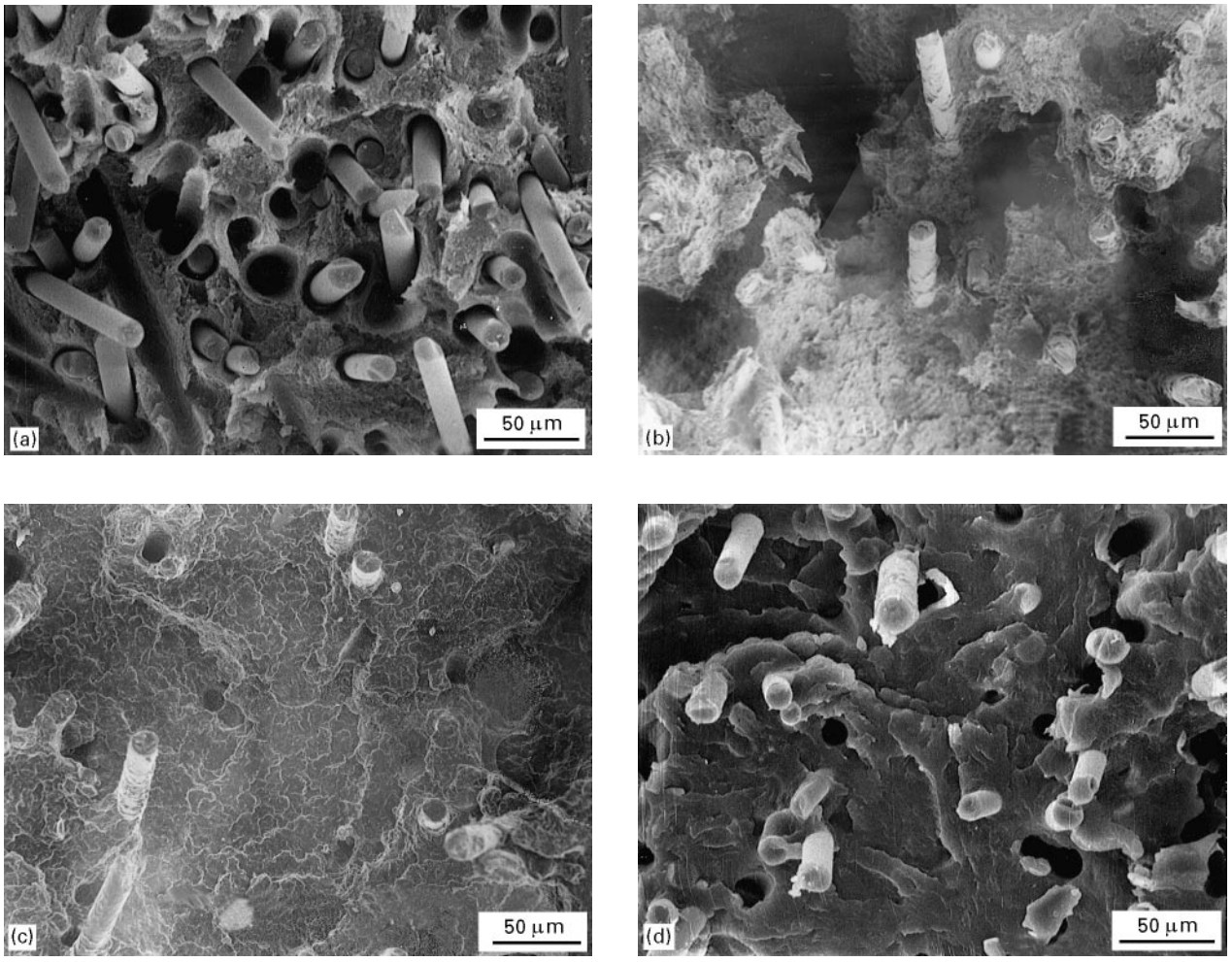

Figure 12 SEM fractographs for the fibre-reinforced materials: (a) pure ABS, (b) 20/80 nylon 6,6/ABS, (c) 80/20 nylon 6,6/ABS and (d) pure nylon.

greater than their unreinforced counterparts. We pointed out in the previous section that enhancement of shear plasticity by fibres hinges on an adequately strong fibre matrix interface. Fracture surfaces for the composite, see Fig. 12, support this. In fibre-reinforced ABS and fibre-reinforced 20/80 nylon 6,6/ABS there was some matrix phase adhering to the fibres but a good portion of the pulled-out fibres showed a clear surface, indicating debonding effects.

Fibres still, however, lowered the toughness relative to the rule-of-mixtures line connecting the toughness of pure ABS with that of pure nylon 6,6 suggesting that damage in the crack-tip zone was a controlling factor in the composites as well. Such damage can be in the form of nylon 6,6/ABS debonding, see Fig. 12, as in the unreinforced materials. It can also be in the form of void formation at the stress concentrated region of fibre ends.

The toughness results for the nylon-rich 80/20 polyblend matrix composite point to a new and beneficial effect of the fibres. Although cavitational plasticity increased relative to shear plasticity in uniaxial tests as a result of fibre additions (see Fig. 8) the toughness of the composite was larger than that of the unreinforced polyblend. The interface here was improved compared to that for the 20/80 case; however, the extent of ABS/nylon debonding was significantly reduced, see fracture surface of Fig. 12c. The composite toughness was still smaller than that given by the rule-of-mixtures line connecting the toughness of pure ABS to pure nylon 6,6 indicating that damage was still present in the composite at crack tips. We conclude that the higher toughness of the composite compared to the corresponding unreinforced blend was the result of less damage overall in the composite at crack tips, when compared to the damage at crack tips in the unreinforced material.

The reduction of ABS/nylon 6,6 debonding at crack tips in the presence of the fibres we attribute to the matrix stress shielding effect of the fibres. Fibres, because of their elongated morphology and high modulus shield the matrix from the applied stresses because more of the applied load is carried by the fibres. In a previous paper [32] we showed that matrix stresses can be lowered by as much as 50% by the stress shielding effect of fibres.

In fibre-reinforced pure nylon 6,6 (Fig. 12d) the fibre/matrix interface was the weakest. There was no matrix phase adhering to the fibres and the fibre surfaces were very clean. Thus we attribute the drastic lowering of the toughness to the formation of extensive fibre/matrix interface debond cracks which then link up with the main crack and thereby reduce fracture initiation toughness.

In summary, fracture initiation toughness was governed by a balance between the enhancement of shear

plasticity by second-phase additions and the embrittlement effects associated with debonding at second-phase/matrix interfaces. The role of fibres and of other rigid polymer phase additions could be understood in the framework of this competing influence of enhanced plasticity and enhanced damage. In the composite, the strength of the fibre/matrix interface was critical in influencing the overall balance between these competing processes. A stronger interface favoured fibre-assisted localized plasticity whereas a weaker interface favoured fibre-induced damage. Also, provided the interface is adequately strong, fibres could have the beneficial effect of alleviating damage in the matrix such as at internal polymer/polymer interfaces by the mechanism of matrix stress shielding.

The above results also provide fundamental insight into the origins of positively synergistic versus negatively synergistic toughening behaviour. As mentioned, for positively synergistic behaviour the toughness lies above the rule-of-mixtures line. Positive synergism was obtained in this blend system when the role of the crack tip was to enhance shear plasticity compared to uniaxial stressing conditions. This was apparently the case in 20/80 nylon 6,6/ABS with a high compatibilizer content, such that damage effects at ABS/matrix interfaces were minimized. Negative synergism was obtained when damage was preferentially induced in the crack-tip region at weak internal interfaces. Fundamentally, then, the objective ought to be to have the strength of polymer/polymer or fibre/polymer interfaces be as high as possible and, further to require that the rubber cavitation stresses be less than the critical debond stresses at the interfaces. In this manner, shear yielding may be preferentially favoured over damage-induced embrittlement at crack tips. A too low critical cavitation stress, however, many not result in adequate enhancement of shear plasticity, as the plastic zone sizes would be too small at low stresses because the volume of the shear yielded zones would be small at low stresses.

3.5. Fracture propagation toughness

In Fig. 13, the overall toughness, J_{ss}, is compared to J_{IC}, for the unreinforced materials. What is notable from this result is that the overall toughness, J_{ss}, could be as much as two to three times the fracture initiation toughness. The exception was pure nylon 6,6 which fractured in a catastrophic manner. This meant that substantial additional toughening is generated during crack advance from a "rising" fracture resistance curve. This significant result has important implications for the use and application of polymer alloys. It points to the fact that such alloys can have acceptable application potential above the conventional initiation toughness, as advocated by standard ASTM tests. This is analogous to the use of metallic alloys above the yield strength as a result of the presence of work hardening or, more recently, the development of creamic composites for applications above the matrix cracking stresses [33]. There is a strong need to develop design methodologies that will exploit this

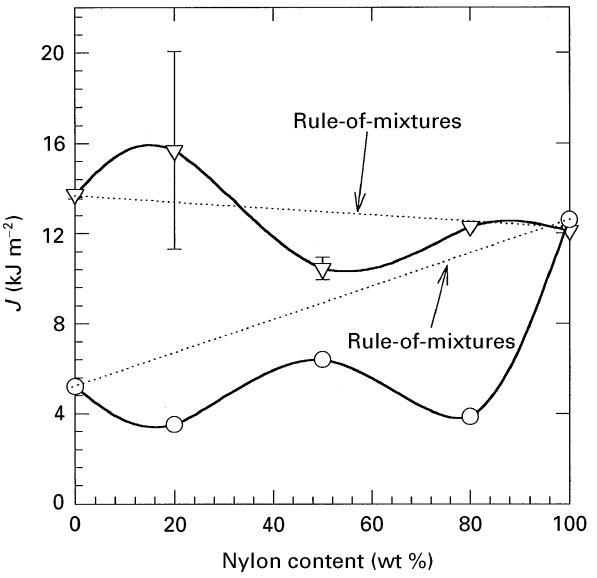

Figure 13 Comparison between (○) the fracture initiation toughness, J_{IC}, and (▽) the plateau value of the fracture resistance, J_{ss}, for the unreinforced alloys at different alloy compositions.

unique capacity of polymeric alloys. This would first require ASTM-type standardization of test procedures for characterizing the *R*-curve potential. The characterization of J_{ss} in this paper is a first step towards this direction.

We note that the J_{ss} values for pure ABS and 20/80 nylon 6,6/ABS were large enough to exceed the plane strain thickness requirement, Equation 1. Consequently, it was not possible unequivocally to determine the role of discontinuous second-phase nylon 6,6 or the exact magnitude of the fracture propagation toughening behaviour of ABS-rich alloys. The indicated values for ABS and 20/80 nylon 6,6/ABS are expected to be plane stress rather than plane strain toughness values. All other J_{ss} values satisfied this plane strain requirement.

There have been two proposed reasons for why there arises a propagation toughness component. One is crack bridging by second phases, either rigid [30] or ductile [34] second phases. In the 20/80 nylon 6,6/ABS as shown in the fracture surface in Fig. 10a, we observed pulled-out nylon 6,6 fibres indicating bridging contribution by the elongated nylon 6,6 phase. Fibre-bridging effects were observed in all composites as can be seen from the pulled-out glass fibres in Fig. 12. The second reason has to do with the closure action of the crack tip plastic zone in the wake of the crack after it has advanced. This second mechanism, which has been both discussed and modelled by Evans *et al.* [35] for the case of rubber-toughened polymers, has not received as much attention.

The role of crack wake plasticity in enhancing crack propagation toughness is supported by the application of a fracture mechanics model of toughening in Part IV [11] of this series. The model was applied to the nylon 6,6/ABS alloys of this study as well as to a nylon 6,6/SAN/rubber system [9, 10] both with and without glass fibres. On the basis of this model, crack wake plasticity appeared to be the primary contributor to the propagation toughening component.

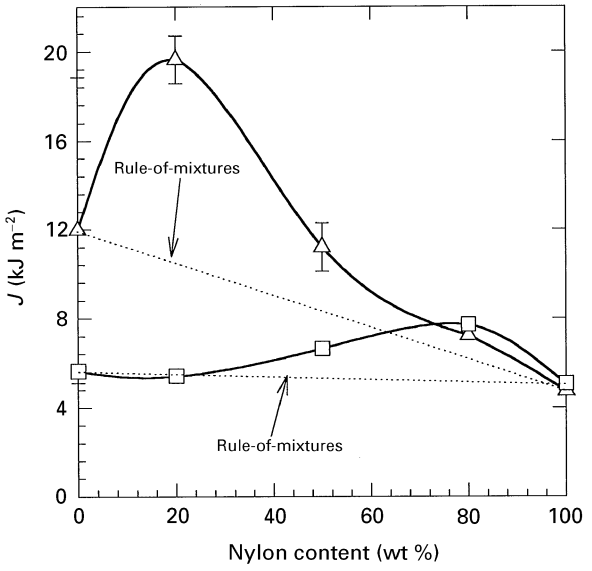

Figure 14 Comparison between (□) the fracture initiation toughness, J_{IC}, and (△) the plateau value of the fracture resistance, J_{ss}, for the fibre-reinforced alloys at different matrix alloy compositions.

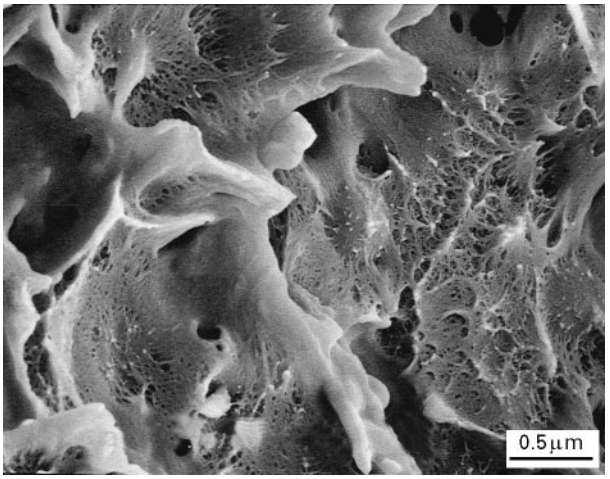

Figure 15 High magnification view in the SEM of the matrix region of the fracture surface of the fibre-reinforced 20/80 nylon 6,6/ABS alloy. Extensive plasticity can be observed in the matrix regions between the fibres.

A secondary component appeared to be crack bridging although this contribution appeared to be small in comparison with wake plasticity. This result has important implications for microstructural design guidelines for polymer alloys and composites. It suggests that microstructures that allow for enhanced localized plasticity in the continuous polymer phase component would not only enhance fracture initiation toughness as discussed above, but would also be the most desirable for propagation toughening.

The absence of crack wake toughening in nylon 6,6 is notable, see Fig. 14, which shows that J_{IC} and J_{ss} were equal for pure nylon 6,6 despite the fact that nylon 6,6 was tough with a larger plastic zone size than some of the other blends with ABS. We offer the following explanation for this. Although in pure nylon 6,6 the specimen failed catastrophically, it did so only after a very small amount of stable crack extension. The absence of a measurable *R*-curve can be related to a specimen geometry effect. If the applied value of J, J_{app}, is greater than the fracture resistance, J_R, then catastrophic failure results. Because the value of J_{app} depends non-linearly on the applied load and the specimen geometry, high toughness material may fail catastrophically simply because J_{app} exceeds J_R once crack advance is initiated. It may be preferable for high toughness materials to use a larger compact tension specimen geometry rather than the small SENB specimens used in this study. This issue is also brought out in the propagation toughening results for the composites below.

The comparison between J_{IC} and J_{ss} for fibre-reinforced polymer alloys are shown in Fig. 14. For the composites, all data points both for J_{ss} and J_{IC}, conformed with plane strain requirements. From the standpoint of the total toughness, J_{ss}, the toughest material was the fibre-reinforced 20/80 nylon 6,6/ABS alloy, wherein $J_{ss} \approx 3$–$4\ J_{IC}$. The high value of J_{ss} in the fibre-reinforced 20/80 nylon 6,6/ABS was consistent with fractographic evidence of enhanced matrix plasticity combined with minimal damage associated with debonding at internal interfaces. Fig. 15, which is a high magnification view of the matrix region of the composite shows a highly plastic matrix, little or no debonding at nylon/ABS interfaces and, as was shown earlier in Fig. 12b an adequately strong fibre/matrix interface.

Fig. 14 also shows, in support of our discussion above for the pure nylon 6,6 case, that although fibre-reinforced 80/20 nylon 6,6/ABS was the toughest composite from the standpoint of fracture initiation toughness, this material possessed no *R*-curve behaviour and hence J_{ss} was equal to J_{IC}. The issue here is similar to that discussed for the pure nylon 6,6 case above. An alternative specimen geometry may need to be utilized to characterize the *R*-curve effect here.

4. Conclusions

1. Addition of ABS to nylon 6,6 changed the deformation mode from primarily deviatoric for pure nylon 6,6 to increasingly dilatational as ABS was introduced. This transition occurred in a roughly linear fashion with volume fraction of ABS. In uniaxial tests, the glass fibres measurably enhanced shear plasticity in the surrounding matrix in the ABS-rich blends but apparently increased dilatational plasticity in the surrounding matrix in nylon-rich blends.

2. Negative synergism in the fracture initiation toughness versus blend composition was obtained both in the unreinforced and in the fibre-reinforced blends primarily because at crack tips damage was initiated in the plastic zone at internal polymer/polymer interfaces and at fibre/polymer interfaces. We demonstrated that the positive synergism would be obtained in an unreinforced blend when the polymer/polymer interface strength is increased.

3. An increase in the fracture initiation toughness was obtained when fibres were added to an alloy matrix. There were apparently two fundamental fibre toughening principles: the first was the tendency to enhance shear plasticity because of the higher

deviatoric stress state in the vicinity of high modulus fibres; the second was the tendency of fibres to shield the matrix from the applied stresses thereby alleviating damage initiation in the surrounding matrix.

4. In both the unreinforced and in the fibre-reinforced polyblends, substantial additional toughening was obtained as a result of crack advance. This toughening appears to derive primarily from the role of the plastic zone in the wake of the advancing crack. Materials with the highest propagation toughening exhibited extensive plasticity and, at the same time, were subjected to minimal distributed damage within the plastic zone. Once again the tendency for fibres to enhance localized plasticity favoured the development of higher crack propagation resistance in the composites compared to the unreinforced alloys.

Acknowledgements

This project was supported by the National Science Foundation under grant MSS-9201625. Support from Monsanto Chemical Company in terms of raw materials, processing facilities and microscopy is acknowledged. The assistance provided by Mr Larry Gustafson for processing, and by Dr Dave Alward for TEM microscopy, is also greatly appreciated.

References

1. H. BREUER, F. HAAF and J. STABENOW, *J. Macromol. Sci. Phys.* **B1** (1977) 387.
2. A. M. DONALD and E. J. KRAMER, *J. Mater. Sci.* **17** (1982) 1765.
3. *Idem*, *ibid.* **17** (1982) 2351.
4. M. E. FOWLER, H. KESKULA and D. R. PAUL, *J. Appl. Polym. Sci.* **35** (1988) 1563.
5. C. B. BUCKNALL, P. S. HEATHER and A. LAZZER, *J. Mater. Sci.* **16** (1989) 2255.
6. R. A. BUBECK, D. J. BUCKLEY, Jr, E. J. KRAMER and H. R. BROWN, *ibid.* **26** (1991) 6249.
7. B. MAJUMDAR, H. KESKULA and D. B. PAUL, *J. Polym. Sci. B Polym. Phys.* **32** (1994) 2127.
8. H.-J. SUE and A. F. YEE, in "ANTEC Conference Proceedings", Vol. 2 (1995) pp. 1517–18.
9. S. V. NAIR, A. SUBRAMANIAM and L. A. GOETTLER, *J. Mater. Sci.* **32** (1997) 5321.
10. *Idem*, *ibid*., submitted.
11. S. V. NAIR and A. SUBRAMANIAM, *ibid*., submitted.
12. L. A. VESTERGAARD, S. V. NAIR and L. A. GOETTLER, *ibid*., submitted.
13. *Idem*, *ibid*., submitted.
14. US Pat. 4713415 (1987).
15. US Pat. 5227428 (1993).
16. R. E. LAVENGOOD and F. M. SILVER, in "ANTEC Conference Proceedings" (1987) p. 1369.
17. *Idem*, in "SPE RETEC Conference Proceedings" (1987) p. 299.
18. D. M. OTTERSON, B. H. KIM and R. E. LAVENGOOD, *J. Mater. Sci.* **26** (1991) 1478.
19. B. MAJUMDAR, H. KESKULA and D. R. PAUL, *Polymer* **35** (1994) 5453.
20. *Idem*, *ibid.* **35** (1994) 5468.
21. B. MAJUMDAR, H. KESKULA, D. R. PAUL and N. G. HARVEY, *ibid.* **35** (1994) 4263.
22. B. MAJUMDAR, H. KESKULA and D. R. PAUL, *ibid.* **35** (1994) 3164.
23. S. V. NAIR, S.-C. WONG, A. SUBRAMANIAM, L.A. GOETTLER and L. A. GUSTAFSON, in "ANTEC Conference Proceedings" (1995) p. 41.
24. B. H. KIM and C. R. JOE, *Engng Frac. Mech.* **34** (1989) 221.
25. T. HASHIDA and V. C. LI, *J. Amer. Ceram. Soc.* **77** (1994) 1553.
26. S. V. NAIR and Y-L. WANG, *J. Amer. Ceram. Soc.* (1995) in press.
27. D. S. PARKER, H.-J. SUE, J. HUANG and A. F. YEE, *Polymer* **31** (1990) 2267.
28. M. L. SHIAO, S. V. NAIR, P. D. GARRETT and R. E. POLLARD, *ibid.* **35** (1994) 306.
29. C. B. BUCKNALL, P. HEATHER and A. LAZZERI, *J. Mater. Sci.* **24** (1989) 1489.
30. S. V. NAIR, M. L. SHIAO and P. D. GARRETT, *ibid.* **22** (1992) 1085.
31. M. L. SHIAO, S. V. NAIR, P. D. GARRETT and R. E. POLLARD, *ibid.* **29** (1994) 1739.
32. S. V. NAIR and S.-C. WONG, ein "ASME Conference Proceedings", Chicago, November 1994 (ASME, New York, 1995).
33. A. G. EVANS, F. ZOK and T. J. MACKIN, in "High Temperature Mechanical Behavior of Ceramic Matrix Composites", edited by S. V. Nair and K. Jakus (Butterworth-Hienneman, Boston, 1995) pp. 3–84.
34. S. KUNZ-DOUGLASS, P W. R. BEAUMONT and M. F. ASHBY, *J. Mater. Sci.* **15** (1990) 1109.
35. A. G. EVANS, Z. B. AHMAD, D. G. GILBERT and P. W. R. BEAUMONT, *Acta Metall.* **34** (1986) 1.

Received 10 October 1996
and accepted 1 May 1997